Research Article | Vol. 24, No. 19 | 19 Sep 2016 | OPTICS EXPRESS 22296

Optics EXPRESS

Low drift cw-seeded high-repetition-rate optical parametric amplifier for fingerprint coherent Raman spectroscopy

JOACHIM KRAUTH,[1,*] TOBIAS STEINLE,[1] BOWEN LIU,[2] MORITZ FLOESS,[1] HEIKO LINNENBANK,[1] ANDY STEINMANN,[1] AND HARALD GIESSEN[1]

[1]*4th Physics Institute and Research Center SCoPE, University of Stuttgart, Pfaffenwaldring 57, 70569 Stuttgart, Germany*

[2]*Ultrafast Laser Laboratory, School of Precision Instruments and Optoelectronics Engineering, Key Laboratory of Optoelectronic Information Technology (Ministry of Education), Tianjin University, Tianjin 300072, China*

[*]*j.krauth@pi4.uni-stuttgart.de*

Abstract: We introduce a broadly tunable robust source for fingerprint (170 – 1620 cm^{-1}) Raman spectroscopy. A cw thulium-doped fiber laser seeds an optical parametric amplifier, which is pumped by a 7-W, 450-fs Yb:KGW bulk mode-locked oscillator with 41 MHz repetition rate. The output radiation is frequency doubled in a MgO:PPLN crystal and generates 0.7 – 1.3-ps-long narrowband pump pulses that are tunable between 885 and 1015 nm with >80 mW average power. The Stokes beam is delivered by a part of the oscillator output, which is sent through an etalon to create pulses with 1.7 ps duration. We demonstrate a stimulated Raman gain measurement of toluene in the fingerprint spectral range. The cw seeding intrinsically ensures low spectral drift.

OCIS codes: (190.4360) Nonlinear optics, devices; (190.4970) Parametric oscillators and amplifiers; (300.6450) Spectroscopy, Raman.

References and links

1. W. J. Tipping, M. Lee, A. Serrels, V. G. Brunton, and A. N. Hulme, "Stimulated Raman scattering microscopy: an emerging tool for drug discovery," Chem. Soc. Rev. **45**(8), 2075–2089 (2016).
2. P. Nandakumar, A. Kovalev, and A. Volkmer, "Vibrational imaging based on stimulated Raman scattering microscopy," New J. Phys. **11**(3), 033026 (2009).
3. Y. Ozeki, W. Umemura, Y. Otsuka, S. Satoh, H. Hashimoto, K. Sumimura, N. Nishizawa, K. Fukui, and K. Itoh, "High-speed molecular spectral imaging of tissue with stimulated Raman scattering," Nat. Photonics **6**(12), 845–851 (2012).
4. C. H. Camp, Jr. and M. T. Cicerone, "Chemically sensitive bioimaging with coherent Raman scattering," Nat. Photonics **9**(5), 295–305 (2015).
5. J. Réhault, F. Crisafi, V. Kumar, G. Ciardi, M. Marangoni, G. Cerullo, and D. Polli, "Broadband stimulated Raman scattering with Fourier-transform detection," Opt. Express **23**(19), 25235–25246 (2015).
6. C. H. Camp, Jr., Y. J. Lee, J. M. Heddleston, C. M. Hartshorn, A. R. Hight Walker, J. N. Rich, J. D. Lathia, and M. T. Cicerone, "High-speed coherent Raman fingerprint imaging of biological tissues," Nat. Photonics **8**(8), 627–634 (2014).
7. I. Pope, W. Langbein, P. Watson, and P. Borri, "Simultaneous hyperspectral differential-CARS, TPF and SHG microscopy with a single 5 fs Ti:Sa laser," Opt. Express **21**(6), 7096–7106 (2013).
8. B. G. Saar, C. W. Freudiger, J. Reichman, C. M. Stanley, G. R. Holtom, and X. S. Xie, "Video-rate molecular imaging in vivo with stimulated Raman scattering," Science **330**(6009), 1368–1370 (2010).
9. J. Mansfield, J. Moger, E. Green, C. Moger, and C. P. Winlove, "Chemically specific imaging and in-situ chemical analysis of articular cartilage with stimulated Raman scattering," J. Biophotonics **6**(10), 803–814 (2013).
10. B. G. Saar, G. R. Holtom, C. W. Freudiger, C. Ackermann, W. Hill, and X. S. Xie, "Intracavity wavelength modulation of an optical parametric oscillator for coherent Raman microscopy," Opt. Express **17**(15), 12532–12539 (2009).
11. D. Zhang, M. N. Slipchenko, D. E. Leaird, A. M. Weiner, and J.-X. Cheng, "Spectrally modulated stimulated Raman scattering imaging with an angle-to-wavelength pulse shaper," Opt. Express **21**(11), 13864–13874 (2013).
12. A. Fast, J. P. Kenison, C. D. Syme, and E. O. Potma, "Surface-enhanced coherent anti-Stokes Raman imaging of lipids," Appl. Opt. **55**(22), 5994–6000 (2016).

#273613 http://dx.doi.org/10.1364/OE.24.022296
Journal © 2016 Received 10 Aug 2016; revised 12 Sep 2016; accepted 13 Sep 2016; published 16 Sep 2016

Optics EXPRESS

13. C. W. Freudiger, W. Yang, G. R. Holtom, N. Peyghambarian, X. S. Xie, and K. Q. Kieu, "Stimulated Raman scattering microscopy with a robust fibre laser source," Nat. Photonics **8**(2), 153–159 (2014).
14. C. Riek, C. Kocher, P. Zirak, C. Kölbl, P. Fimpel, A. Leitenstorfer, A. Zumbusch, and D. Brida, "Stimulated Raman scattering microscopy by Nyquist modulation of a two-branch ultrafast fiber source," Opt. Lett. **41**(16), 3731–3734 (2016).
15. R. Selm, M. Winterhalder, A. Zumbusch, G. Krauss, T. Hanke, A. Sell, and A. Leitenstorfer, "Ultrabroadband background-free coherent anti-Stokes Raman scattering microscopy based on a compact Er:fiber laser system," Opt. Lett. **35**(19), 3282–3284 (2010).
16. T. Steinle, V. Kumar, M. Floess, A. Steinmann, M. Marangoni, C. Koch, C. Wege, G. Cerullo, and H. Giessen, "Synchronization-free all-solid-state laser system for stimulated Raman scattering microscopy," Light Sci. Appl. **5**, e16149 (2016).
17. T. Steinle, V. Kumar, A. Steinmann, M. Marangoni, G. Cerullo, and H. Giessen, "Compact, low-noise, all-solid-state laser system for stimulated Raman scattering microscopy," Opt. Lett. **40**(4), 593–596 (2015).
18. F. Mörz, T. Steinle, A. Steinmann, and H. Giessen, "Multi-Watt femtosecond optical parametric master oscillator power amplifier at 43 MHz," Opt. Express **23**(18), 23960–23967 (2015).
19. H. Linnenbank and S. Linden, "High repetition rate femtosecond double pass optical parametric generator with more than 2 W tunable output in the NIR," Opt. Express **22**(15), 18072–18077 (2014).
20. B. Köhler, U. Bäder, A. Nebel, J.-P. Meyn, and R. Wallenstein, "A 9.5-W 82-MHz-repetition-rate picosecond optical parametric generator with cw diode laser injection seeding," Appl. Phys. B **75**(1), 31–34 (2002).
21. H. Linnenbank, T. Steinle, and H. Giessen, "Narrowband cw injection seeded high power femtosecond double-pass optical parametric generator at 43 MHz: Gain and noise dynamics," Opt. Express **24**(17), 19558–19566 (2016).
22. J. M. O. Daniel, N. Simakov, M. Tokurakawa, M. Ibsen, and W. A. Clarkson, "Ultra-short wavelength operation of a thulium fibre laser in the 1660-1750 nm wavelength band," Opt. Express **23**(14), 18269–18276 (2015).
23. A. Steinmann, B. Metzger, R. Hegenbarth, and H. Giessen, "Compact 7.4 W femtosecond oscillator for white-light generation and nonlinear microscopy," in *Proceedings of CLEO 2011* (Optical Society of America, 2011), paper CThAA5.
24. M. Tokurakawa, J. M. O. Daniel, C. S. Chenug, H. Liang, and W. A. Clarkson, "Wavelength-swept Tm-doped fiber laser operating in the two-micron wavelength band," Opt. Express **22**(17), 20014–20019 (2014).
25. J. Konradi, A. K. Singh, and A. Materny, "Mode-focusing in molecules by feedback-controlled shaping of femtosecond laser pulses," Phys. Chem. Chem. Phys. **7**(20), 3574–3579 (2005).
26. M. A. Marangoni, D. Brida, M. Quintavalle, G. Cirmi, F. M. Pigozzo, C. Manzoni, F. Baronio, A. D. Capobianco, and G. Cerullo, "Narrow-bandwidth picosecond pulses by spectral compression of femtosecond pulses in second-order nonlinear crystals," Opt. Express **15**(14), 8884–8891 (2007).

1. Introduction

Coherent Raman imaging methods are emerging tools in life sciences due to their large potential in label-free, high speed imaging with applications such as medical diagnostics, the minimally invasive study of cellular metabolism, and drug delivery [1]. Currently, coherent anti-Stokes Raman scattering (CARS) and stimulated Raman scattering (SRS) are vastly being investigated and have originated a diverse field of technologies ranging from narrowband single-frequency [2, 3] to hyperspectral methods [4–7]. The two spectral regions that are of major importance for coherent Raman spectroscopy (CRS) span from 500 – 1700 cm^{-1} ("fingerprint") and 2700 – 3300 cm^{-1} ("CH-stretch"). The latter provides strong vibrational signals, which has enabled video-rate CARS and SRS imaging of biological tissue [8]. The fingerprint region, in contrast, enables superior chemical specificity, but shows weaker signal and is thus more demanding for the driving light source.

Narrowband CRS requires a dual-beam light source with tunable frequency difference to match the molecular vibration frequencies. The light source should provide nJ-level pulse energy and pulse durations in the 1 – 2 ps range. The vast majority of work over the past decade has been obtained by using optical parametric oscillator (OPO) technology [9–12]. However, OPOs are sensitive to ambient and pumping conditions, which make them difficult to handle. Hence, stabilized and automated versions require extensive monitoring and active control mechanisms, which increases complexity and cost. Recently, more robust synchronized Er- and Yb-doped fiber laser systems have been introduced for imaging in the CH-stretch region [13–15]. The use of fiber oscillators, though, comes at the cost of more sophisticated detection schemes, i.e., autobalanced detection [13]. Transfer to the fingerprint region is not straightforward due to the lack of gain media. Recently, we have demonstrated that cw-seeding of optical parametric amplifiers (OPAs) is a viable alternative to these

Optics EXPRESS

techniques, by combining the simplicity and robustness of the OPA concept with ultra-low intensity noise of solid-state oscillators [16, 17]. There are, however, no suitable tunable semiconductor gain media commercially available to straightforwardly transfer the concept to the fingerprint. Further, the parametric single-pass gain for 1-µm-pumped systems is lower in this spectral region, due to group velocity mismatch [18].

We overcome these issues by using a Tm-doped fiber laser to provide the tunable cw-seed in the 1770 – 2030 nm range and an oscillator-pumped double-pass OPA [19–21] for power scaling. Furthermore, the second harmonic generation (SHG) of the OPA output is used as Raman pump beam in SRS, and the low-noise 1033 nm pulse from an Yb:KGW oscillator is used as Stokes beam. Generally, the use of an OPA system for SRS measurements brings about numerous advantages, such as being scalable and compatible with flexible repetition rate in both directions. In addition, it is insensitive to minor changes of the environmental conditions. Lastly, a step-by-step optimization is possible; hence it offers easy handling and troubleshooting.

2. Experimental setup

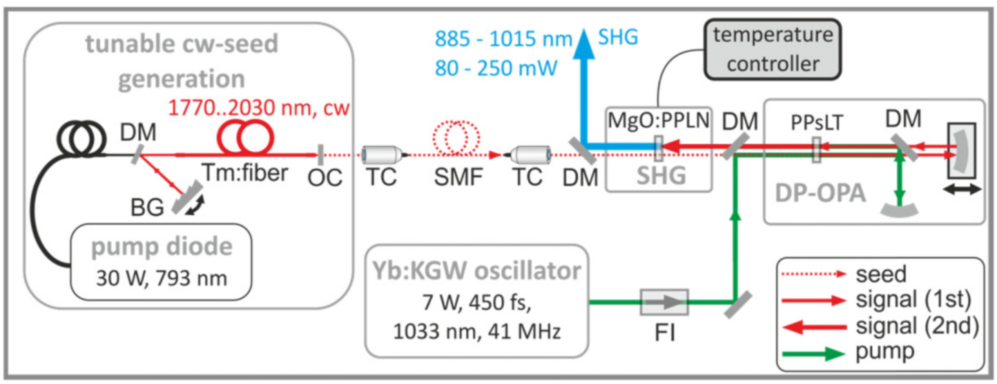

Fig. 1. Schematic diagram of the experimental setup of the TDFL seeded double-pass OPA and subsequent SHG. OC: output coupling mirror; BG: blazed grating; TC: triplet collimator; SMF: single mode fiber; PPLN: periodically-poled lithium niobate; PPsLT: periodically-poled stoichiometric lithium tantalate; DM: dichroic mirror; FI: Faraday isolator.

Figure 1 depicts the experimental setup. The thulium-doped fiber laser (TDFL) is based on a linear resonator configuration and cladding-pumped by a 30 W fiber-coupled diode (Dilas Diodenlaser GmbH) with a diameter of 100 µm at 793 nm. The pump laser is collimated and launched into the active fiber by two aspheric lenses with focal lengths of 11 mm. The thulium-doped fiber (Nufern Inc., LMA-TDF-25P/250-LC) has a core/cladding diameter of 25/250 µm, a numerical aperture of 0.09/0.46, and a low thulium doping concentration. The Tm-fiber is 11 cm long, so that low doping concentration and short fiber length ensure the output wavelength to be tuned to the shorter wavelength range [22]. For sufficient cooling of the active fiber, the thulium-doped fiber is spliced to a 20-cm-long passive fiber with 25 µm, 0.1 NA core and 0.36 NA, 250 µm cladding (Nufern Inc., MM-GDF-25/250-11FA). Then, the fiber was mounted in a water-cooled temperature-stabilized V-groove copper heat sink to prevent thermal damage. In addition, cooling is advantageous for low wavelength generation. A dichroic mirror (DM) combines the signal laser and pump laser and reflects the signal laser to a blazed grating (1200 lines/mm) arranged in Littrow configuration to provide stable wavelength selective feedback. The 10% output coupler is placed directly at the facet of the passive fiber for stable beam pointing.

The generated output of the TDFL is collimated by a 10x objective and is coupled into a single mode fiber with a triplet collimator. It is used as seed for the OPA, which is based on an 11-mm-long PPsLT crystal as nonlinear gain medium. It is designed in a fan-out manner

Optics EXPRESS

and offers poling periods between 29.3 to 32.4 µm. The PPsLT crystal is uncoated, resulting in reflection losses of 14% per surface. An Yb:KGW oscillator [23] is used as pump source for the OPA. It delivers up to 7 W average output power at 41 MHz repetition rate and 450 fs pulse duration at a central wavelength of 1033 nm. Pump and seed beam are combined using a DM (long-pass filter 1400 nm). The OPA is designed in a double-pass configuration [19], where OPA signal and pump are separated with another DM (long-pass filter 1400 nm) and are both reflected back using curved mirrors with a radius of curvature of 200 mm for the second pass through the PPsLT crystal. To adjust the temporal overlap between pump and signal for the second OPA pass a delay stage is added. The residual pump beam is sent back into a Faraday isolator.

The generated signal beam of the two-stage OPA is reflected back in the opposite direction of the incident seed and focused into a 10-mm-long MgO:PPLN crystal with poling periods between 24.06 and 36.95 µm which is designed for SHG from 860 to 1350 nm. The incident surface of the MgO:PPLN crystal is anti-reflection coated for the OPA signal (T>96%), while the other surface is uncoated resulting in reflection losses of 14%. To achieve phase-matching for the different wavelengths, the MgO:PPLN crystal is mounted in a temperature-controlled oven. Finally, the generated SHG pulses are separated from the OPA signal using another DM (long-pass filter 1400 nm).

3. Experimental results

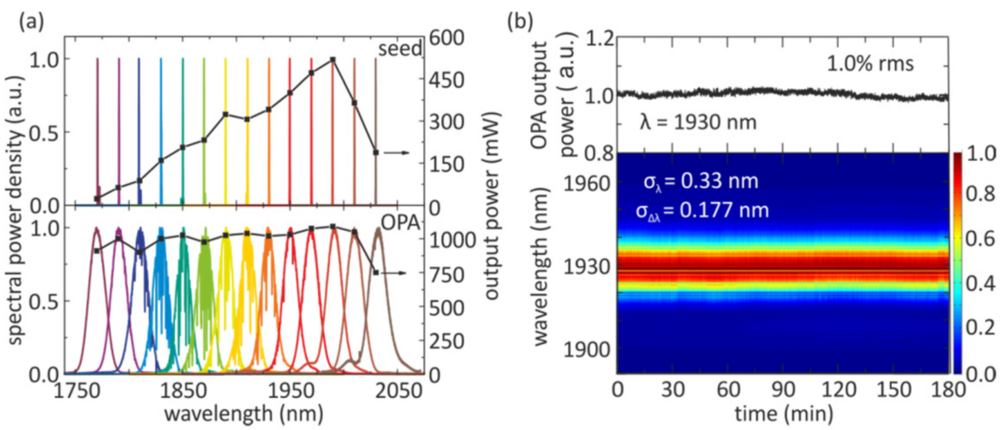

Fig. 2. (a) Power and spectra of the TDFL seed (top) and double-pass OPA (bottom). The tuning range spans from 1770 – 2030 nm. Figure (b) depicts the long term average output power (top) and spectral (bottom) stability of the OPA taken at 1930 nm over a measurement time of 3 h. The OPA reaches 1.0% rms passive power stability in 3 h, as well as a standard deviation of the central wavelength of 0.33 nm, while the spectral bandwidth varies by 0.177 nm at a FWHM of 14.3 nm.

By changing the angle of incidence on the grating in the TDFL, the output laser wavelength is tuned from 1770 – 2030 nm, as depicted in the upper panel of Fig. 2(a). Of the more than 100 mW generated cw seed power, typically 30 mW are used to seed the two-stage OPA. Due to the tunable output wavelength of the TDFL, a gap-free tuning range of the OPA is realized from 1770 – 2030 nm, in which the OPA average power is almost constant with about 1 W when 4 W of pump power is applied, as shown in the lower panel of Fig. 2(a). This corresponds to a photon conversion efficiency of up to 50%. In the 1800 – 1950 nm range, atmospheric absorption is visible in the OPA spectra. Wavelength tuning is performed by tuning the seed wavelength; for larger steps ($\Delta\lambda$>10 nm) the lateral position of the PPsLT crystal, and hence the phase-matching condition were adjusted accordingly.

The cw TDFL [24] is designed in Littrow configuration, resulting in high wavelength stability. Due to the low drift of solid-state oscillators, the free-running spectral and power stability of the OPA is very high, as shown in Fig. 2(b). During a measurement time of 3 h a passive power stability of 1.0% rms is obtained without further stabilization. The measurement has been taken exemplarily at 1930 nm. The standard deviation of central wavelength is 0.33 nm with 0.017% rms. In addition, the spectral bandwidth (FWHM) of 14.3 nm shows a standard deviation of 0.177 nm and 1.264% rms; moreover, a spectral drift as low as 0.28 nm/h is recorded. Hence, our system provides enough spectral stability for demanding applications.

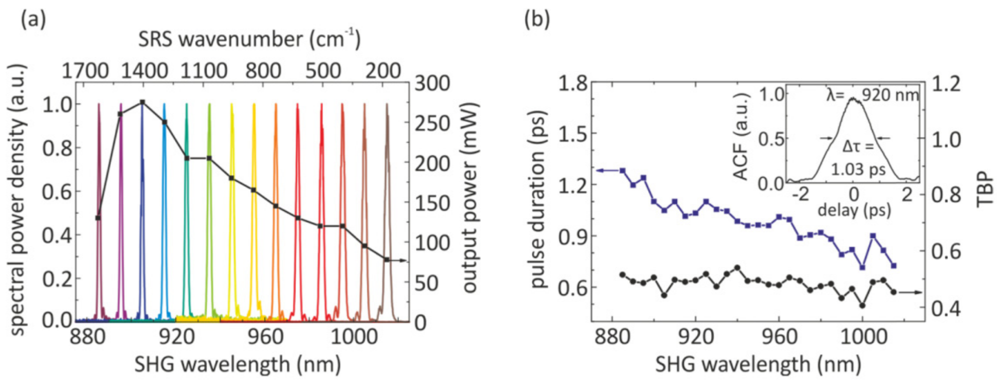

Fig. 3. (a) Power and spectra of second harmonic and respective SRS wavenumber using the Yb:KGW oscillator at 1033 nm for the generation of the Stokes beam. The tuning range spans from 885 – 1015 nm. Figure (b) displays the SHG pulse duration and time-bandwidth-product (TBP) as a function of wavelength. The inset in (b) shows exemplarily the autocorrelation trace at a central SHG wavelength of 920 nm.

Figure 3(a) shows the tuning range of the last stage of our experimental setup, namely the second harmonic generation. Here, the tuning range spans according to the OPA tuning range from 885 – 1015 nm, corresponding to a pump-Stokes frequency detuning from 170 – 1620 cm^{-1} using 1033 nm as Stokes wavelength. Tuning is performed by changing the poling period as well as the temperature of the MgO:PPLN crystal and adjusting the seed wavelength for maximum SHG power output. Additionally, in Fig. 3(a) the SHG power is displayed, which exhibits a maximum power of 270 mW at a wavelength of 900 nm. Over 80 mW are available in the entire tuning range. We observe a bandwidth of 1.0 – 2.6 nm (12 – 27 cm^{-1}) with broader spectra at longer SHG wavelengths. Due to the fixed temperature of the nonlinear crystal set by the temperature controller, the SHG wavelength is spectrally very stable. Furthermore, Fig. 3(b) shows the pulse duration and the time-bandwidth-product (TBP) of the SHG pulses as a function of wavelength. Assuming a sech^2 pulse shape, pulse durations between 0.7 and 1.3 ps have been measured, while longer pulses are obtained at shorter wavelengths. However, the TBP stays almost constant over the entire tuning range at around 0.5 due to the increasing spectral bandwidth of the SHG pulses. The inset of Fig. 3(b) shows exemplarily the autocorrelation taken at 920 nm SHG wavelength. In addition, the beam profile of the SHG pulses was examined to be close to the fundamental TEM_{00} mode.

Finally, our tunable picosecond laser system was applied to fingerprint coherent Raman spectroscopy of toluene (C_7H_8). Figure 4(a) illustrates our measurement setup. The tunable SHG of the two-stage OPA is employed as pump beam, while the pulses from the Yb:KGW oscillator are used as Stokes beam. This results in a measurement range in the fingerprint region from 170 – 1620 cm^{-1}. However, the employed optics restrict the measurement range to the 400 – 1550 cm^{-1} range. The fixed frequency 1033 nm Stokes pulses are created from the residual oscillator power by spectral filtering using an etalon with a free spectral range of 85 cm^{-1} and a finesse of 12, resulting in pulses with 8 cm^{-1} bandwidth and a pulse duration of 1.7 ps. The pump power was 75 mW, whereas the Stokes power was 10 mW. Pump and Stokes pulses are synchronized by a delay line, collinearly combined by a DM (short-pass

Optics EXPRESS

1000 nm) and focused into the toluene sample. The transmitted light is collected with an achromatic lens while a long-pass filter separates the Stokes from the pump beam. We detect the stimulated Raman gain (SRG) of the Stokes beam, which benefits from the extremely good noise properties of the Yb:KGW oscillator. An acousto-optic modulator (AOM) is used to modulate the pump pulses at 1 MHz, while the Stokes intensity is detected by a single-channel amplified silicon photodiode, which is connected to a high-frequency lock-in amplifier.

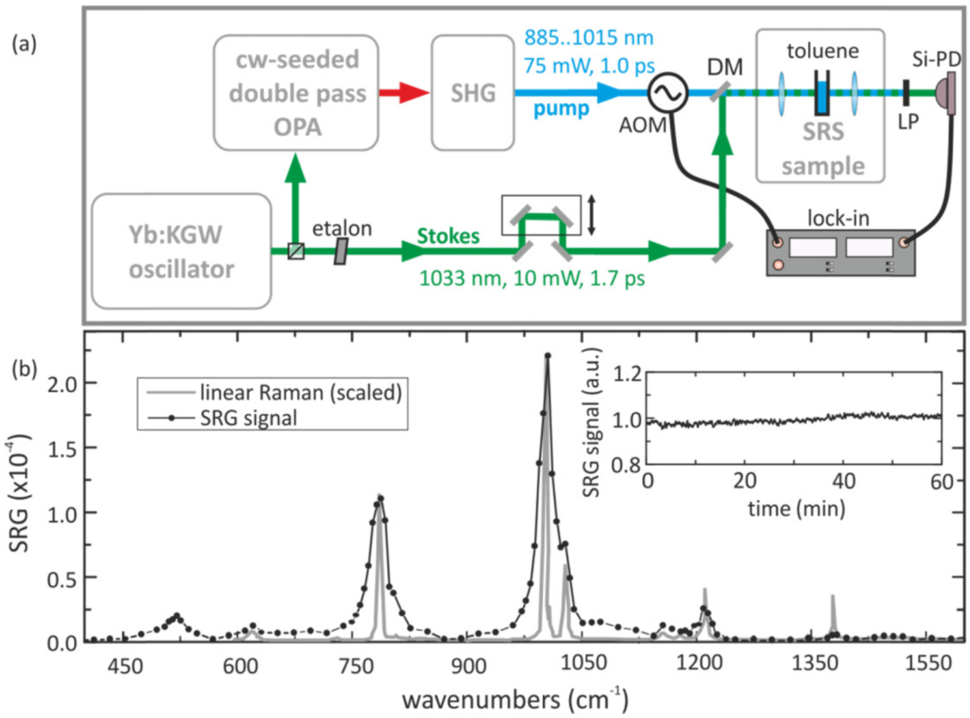

Fig. 4. (a) Schematic diagram of the experimental SRS setup. The output of the TDFL seeded double-pass OPA is frequency-doubled and used as the pump beam, while the Yb:KGW oscillator delivers the Stokes beam. AOM: acousto-optic modulator; DM: dichroic mirror; LP: long-pass filter; Si-PD: amplified silicon photo diode. (b) Measured SRG spectrum of toluene with reference data in the fingerprint region (400 – 1550 cm^{-1}). The inset in (b) shows the SRG signal stability measurement taken at the maximum SRG peak at 1003 cm^{-1} over 60 min.

The resulting SRG spectrum can be seen in Fig. 4(b), which is plotted in comparison to a literature value obtained from [25]. Except for the peak at 1400 cm^{-1} the relative height of the SRG peaks match the literature data. The mismatch at 1400 cm^{-1} might be caused by the narrowband resonance, relatively long SHG pulses around 900 nm leading to lower peak power and hence lower SRS signal, or beam pointing issues. The other peaks are at the same spectral position, while every peak is detected. In addition to the peaks covered by the literature data, which spans from 600 – 1600 cm^{-1}, an additional peak at 525 cm^{-1} is observed. However, due to the broad bandwidth of our pump pulses (12 – 27 cm^{-1}) the SRG spectrum is somewhat smeared out. This effect can be minimized using a longer nonlinear crystal [26] and hence matching the bandwidth of pump and Stokes beam.

Moreover, the inset of Fig. 4(b) illustrates the stability of the SRG signal, measured as a function of time over a period of 60 min taken at a central pump wavelength of 936 nm, corresponding to a SRS wavenumber of about 1003 cm^{-1} at the highest peak of the toluene SRG spectrum. The measurement indicates a slight drift to higher intensity at a rate of 3.5% per hour. We found the beam pointing of the SRS setup due to temperature changes to be the

Optics EXPRESS

limiting factor, thus the stability can be improved by minimizing the optical path lengths in the setup.

4. Conclusion

In conclusion, we have demonstrated a low-drift TDFL seeded double-pass OPA and proved its applicability to fingerprint SRS spectroscopy. The approach combines the high tunability of a TDFL with the simplicity of an OPA. Our system is capable of providing gap-free tunable output pulses from 885 – 1015 nm with up to 270 mW, leading to an SRS tuning range from 170 – 1620 cm^{-1}. We have shown that the system is operating at a stable performance in measuring the SRS signal over a period of 60 min. The cw-seeding concept supports variable repetition rates and pulse durations of the pump laser, making the system very flexible. The use of shorter pump pulses would increase the spectral bandwidth generated in the OPA and hence support broadband CRS techniques. A next step to improve the current setup could be the implementation of a longer PPLN crystal for spectral narrowing of the pump pulses and hence increasing the spectral resolution of the SRS measurement. Furthermore, by using a more compact all-fiber TDFL or an external cavity diode laser this setup could be further simplified.

Funding

European Research Council Advanced Grant COMPLEXPLAS (501100000781); Deutsche Forschungsgemeinschaft (501100001659); Bundesministerium für Bildung und Forschung (501100002347); Carl-Zeiss-Stiftung (100007569); Baden-Württemberg Stiftung (100008316).

Acknowledgments

We acknowledge support from the open access fund of University of Stuttgart.